Paper was published on **20th October 2023** in

Multiscale and Multidisciplinary Modeling, Experiments and Design,

DOI & the official published version of text will be updated **soon.**

Design of fractional order multistage controller for frequency control improvement of a multi microgrid system using equilibrium optimizer

Satyajeet Das, Pratap Chandra Nayak, Ramesh Chandra Prusty*, Sidhartha Panda
Department of Electrical Engineering, VSSUT, Burla 768018, Odisha, India
*Corresponding author e-mail: ramesh.prusty82@gmail.com, Phone: +91-9439394375

Abstract

This article suggests a Fractional Order multistage (FOPID/ (1+PI)) controller for the improvement of frequency regulation of two interconnected microgrids (MG) systems. The scaling of the suggested controllers is done using a novel meta-heuristic equilibrium optimizer (EO) algorithm which has robust exploitation and exploration proficiencies. The two interconnected microgrid systems comprise various renewable sources such as wind generation systems, photovoltaic (PV) arrays, and diesel generators with various energy storage units. The real wind dynamics and solar irradiance measured values are used for the modelling of wind and PV systems. In the microgrid system, the unpredictability of solar, wind, and load demand creates complicacy in performance which is reflected in frequency oscillations. As a result, power balance among generators must be established by building a robust controller for load frequency regulation (LFC). The frequency responses of the MG with PID controller and fractional-order PID (FOPID) controller are compared to demonstrate the efficacy of the cascaded controller i.e., FOPID/ (1+PI) controller. To demonstrate the superiority of EO, its results are compared with the most prevalent algorithms, and a sensitivity analysis is performed to illustrate its adaptability.

Keywords

Load Frequency Control, Microgrid, Electric Vehicles, Ultra-Capacitor, Fractional-order cascade controller, Equilibrium Optimizer.

1. Introduction

From the point of view of power production and circulation, it is not practicable to provide electricity from the utility grid to remote areas. In this context, a standalone MG system is capable of supplying electrical power to meet the electrical demands of various remote consumers [1]. Microgrids are capable of conveying power collected from distributed generation sources to local loads and utility grids in islanded mode and grid-connected mode respectively. Due to variations in load or the presence of unanticipated uncertainties, such as wind and PV systems, an imbalance of power occurs between the total generation and the total demand in the standalone mode operation. As a result, microgrid performance is insecure, particularly in terms of active power and frequency. Though electric vehicles (EV), microturbine MT, and ultra-capacitors (UC) may partially adjust for both aberrations the whole system is highly unstable. In a standalone microgrid system, frequency control is essential to ensure system performance stability [2]. The foremost goal of frequency control is to keep it within a tolerable range to manage demand fluctuations and disturbance [3]. To accomplish this persistence, diverse approaches such as hearty control [4], shaft moving control [5], and decentralized angle control [6] have been projected by various researchers. However, these methods have a few flaws that make them difficult to implement. As a result, numerous researchers suggest some new adaptive approaches, such as fuzzy logic (FL) [7] and neural networks (NN) [8] based on artificial intelligence (AI). Although these adaptive

approaches are capable of handling the power system's nonlinearities. An adaptive fuzzy approach [9] scaled through a hybrid moth flame pattern search has been used to improve diverse system frequency stability. Fractional-order (FO) controllers [10] have gained popularity in recent years due to improvements in adaptability [11]. With the integration of intelligent approaches [12], such as fuzzy methodology [13] and neural network (NN), fractional-order controllers are demonstrating outstanding performance. The FO control has been applied to gain control of 2dof helicopters [14], frequency control in multiarea microgrids [15], restructured energy systems [16], and power system stabilizers [17] are only a few of the applications for these combinations. Researchers applied fractional computation control [18] for discrete power output and storage in an integrated RES system. The FOPID control setup was used as a secondary frequency controller for an islanded microgrid [19], and the results were better than those produced by the fractional controller. A double-stage cascaded controller [20] is designed for LFC issues, where the first stage is the proportional derivative with filter (PDF) controller which increases the transient characteristic while neutralizing the influence of the D controller's derivative kick. The (1+PI) controller improves performance by lowering errors in the next step. This prompted the use of a fractional-order-based cascaded PI controller for MG systems, namely (FOPID/ (1+PI)).

In the related literature, many researchers have used eclectic algorithms of different types to solve the problem of frequency regulation. The genetic algorithm (GA) [21] used in 2-area-interconnected systems, particle swarm optimization (PSO) and gravitational search algorithm [22] are used to improve PSS and SSSC performance. The Cuckoo search algorithm [23], firefly algorithm [24], Sunflower Algorithm [25], Grasshopper optimisation algorithm [20], Imperialist competitive algorithm (ICA) [26], etc. implemented to set the controller parameters for the improved power system performance. A hybrid whale optimization algorithm with simulated annealing [27] has been employed to scale FO-based type 2 fuzzy variables to provide appropriate damping towards nonlinear disturbances encountered in an integrated system. A recurrent NN-based predictive control [28] was suggested for PV-diesel microgrid systems for frequency stability. A marine predator algorithm (MPA) [29] has been employed to set a fuzzy-PIDF controller to overcome disturbances resulting from renewable energy penetration. Even though such algorithms provide greater execution for the design problem, they still suffer from a long time to run, a tendency to become stuck in local optima, and so on.

The EO is a newly developed physics-based optimization procedure for a control volume [30], which drew inspiration from a general mass balance equation. This research employs EO to modify solutions at random using its high exploratory and exploitative search processes. As a result, the current article has focused on an EO-based (FOPID/ (1+PI)) controller for a multi-area MG.

The key contributions are listed below:

1) The modelling multi-area microgrid system with a wind generation system, PV arrays, diesel generators, and microturbines (MT) incorporating storage devices like fuel cells (FC), electric vehicles (EV), and ultra-capacitors (UC).
2) The work recommends a robust fractional order cascaded controller (FOPID/(1+PI)) to maintain frequency stability in the MMG in the face of a variety of uncertainties (variation in load, variation in wind, and disparity in solar intensity).
3) To design an optimized FOPID controller in diverse operation zones, an innovative cosine-sine approach called equilibrium optimizer (EO) is provided, intensified by the universal weight balance equation for a control issue.

4) Different comparative studies have been provided to support the viability of the proposed EO method over various intelligent optimization algorithms such as GA, PSO, and sine-cosine algorithm (SCA).
5) The anticipated FOPID/ (1+PI) controller's effectiveness is demonstrated by a thorough comparison of the PID and FOPID controllers.
6) The robustness of the anticipated EO-based FOPID(1+PI) controller is vindicated by sensitivity analysis followed by system parameter alternation, removal of micro sources and time-delay analysis.

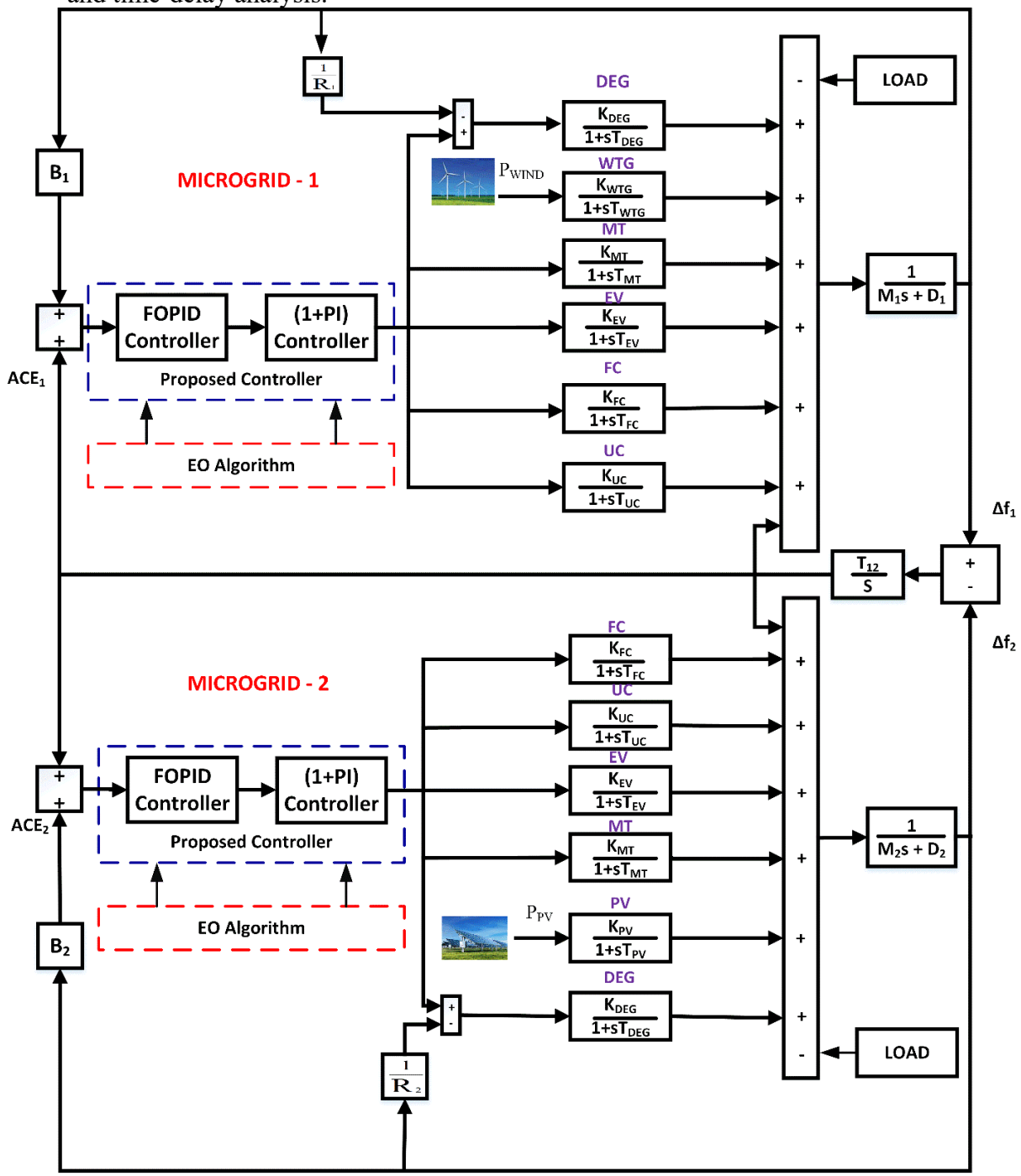

Fig 1: The 2-area MG system model

2. System Under Study

The multiarea microgrid system considered in the study consists of a wind generation system, diesel generators, microturbine (MT), fuel cell (FC), electric vehicle (EV) and ultracapacitor (UC) in respectively area-1 and diesel generators, PV arrays, MT, FC, EV and UC respectively in area-2 as shown in Fig. 1. The positive (+) symbol in the two-area model denotes supplying power to the MG system, while the negative (-) symbol denotes absorbing power from the MG system. The elements of MG are mathematically represented below:

2.1 Diesel Engine Generator (DEG)

DEG's transfer function model is as follows:

$$G_W(\mathrm{s}) = \frac{\Delta P_{DEG}(s)}{\Delta P_D(s)} = \frac{K_{DEG}(s)}{1+sT_{DEG}(s)} \quad (1)$$

Where, ΔP_D = variation in DEG input power, ΔP_{DEG} = variation in DEG output power, T_{DEG} = DEG'S time constant, K_{DEG} = DEG's gain.

2.2 Wind Turbine Generator (WTG)

WTG's transfer function model is as follows:

$$G_W(\mathrm{s}) = \frac{\Delta P_{WTG}(s)}{\Delta P_W(s)} = \frac{K_{WTG}(s)}{1+sT_W(s)} \quad (2)$$

Where, ΔP_W = variation in WTG input power, ΔP_{WTG} = variation in WTG output power, T_{WTG} = WTG's time constant, K_{WTG} = WTG's gain.

2.3 Photo Voltaic cell (PV)

PV's transfer function model is as follows:

$$G_{PV}(\mathrm{s}) = \frac{\Delta P_{PV}(s)}{\Delta P_{\emptyset}(s)} = \frac{K_{PV}(s)}{1+sT_{PV}(s)} \quad (3)$$

where ΔP_Φ = variation in PV input power, ΔP_{PV} = variation in PV output power, T_{PV}= PV's time constant, K_{PV} = PV's gain.

2.4 Micro Turbine (MT)

MT's transfer function model is as follows:

$$G_{MT}(\mathrm{s}) = \frac{\Delta P_{MT}(s)}{\Delta P_M(s)} = \frac{K_{MT}(s)}{1+sT_{MT}(s)} \quad (4)$$

where ΔP_M = variation in MT input power, ΔP_{MT} = variation in MT output power, T_{MT} = time constant of MT system, K_{MT} = MT's gain.

2.5 Fuel Cell (FC)

FC's transfer function model is as follows:

$$G_{FC}(\mathrm{s}) = \frac{\Delta P_{FC}(s)}{\Delta P_F(s)} = \frac{K_{FC}(s)}{1+sT_{FC}(s)} \quad (5)$$

Where, ΔP_F = variation in FC input power, ΔP_{FC} = variation in FC output power, T_{FC} = FC's time constant, K_{FC} = FC's gain.

2.6 Electric Vehicle (EV)

EV's transfer function model is as follows:

$$G_{EV}(\mathrm{s}) = \frac{\Delta P_{EV}(s)}{\Delta P_E(s)} = \frac{K_{EV}(s)}{1+sT_{EV}(s)} \quad (6)$$

Where, ΔP_E = variation in EV input power, ΔP_{EV} = variation in EV output power, T_{EV} = EV's time constant, K_{EV} = EV's gain.

2.7 Ultra Capacitor (UC)

UC's transfer function model is as follows:

$$G_{UC}(s) = \frac{\Delta P_{UC}(s)}{\Delta P_U(s)} = \frac{K_{UC}(s)}{1+sT_{UC}(s)} \quad (7)$$

Where, ΔPU = variation in UC input power, ΔPUC = variation in UC output power, TUC = U C's time constant, KUC = UC's gain.

2.8 Power/ Frequency Eccentricity

To provide dependable electricity, the generated power is required to be properly controlled and must produce stable productivity. However, the behaviour of RES is unpredictable. As a result, the power regulation structure is anticipated to eradicate the deviation of power supply (P_S) and the required load (P_L). The power regulation structure is achieved by the following condition as shown below:

$$\Delta P_e = P_s - P_L \quad (8)$$

The total power generated by the components of the described model is denoted by Ps, while the desired demand is denoted by PL. Frequency fluctuations are caused by the net power deviation. The model frequency deviation (Δf) is calculated in this way.

$$\Delta f = \frac{\Delta P_e}{\Delta K_{sys}+D} \quad (9)$$

The system frequency characteristics constant, K_{sys}, is a constant that represents the system's frequency characteristics. As a result, the model's transfer function representation is represented as

$$G_{SYS}(s) = \frac{\Delta f}{\Delta P_e} = \frac{1}{Ms+D} \quad (10)$$

Which, D = 0.12 and M = 0.2 are the suggested MG system's corresponding damping coefficient and inertia coefficient, respectively. The droop constant is set to 0.5 in this article. The biasing factor of frequency is 20.12 and the synchronous coefficient is taken to be 1.4. Figure 1 depicts the proposed MMG system's model.

Table 1: The MMG model parameters

COMPONENTS	GAIN (*K*)	TIME CONSTANT (*T*)
DEG	$K_{DEG} = 1$	$T_{DEG} = 2$
WTG	$K_{WTG} = 1$	$T_{WTG} = 1.5$
PV	$K_{PV} = 1$	$T_{PV} = 1.8$
MT	$K_{MT} = 1$	$T_{MT} = 2$
FC	$K_{FC} = 0.01$	$T_{FC} = 4$
EV	$K_{EV} = 0.01$	$T_{EV} = 0.2$
UC	$K_{UC} = 7$	$T_{UC} = 0.9$

3. Anticipated Methods

3.1 Cascaded (FOPID/(1+PI)) Controller

In comparison to conventional controllers, fractional-order (FO) controllers offer an additional set of parameters and effective outcomes with a high degree of accuracy with non-minimal phase systems. The integral portion, on the other hand, improves the steady-state response in a normal PID controller. On the other side, it causes delayed system responsiveness and reduces relative stability. The derivative component improves dynamic response, accelerates the system, and increases stability. Furthermore, it increases the system's sensitivity to noisy disruptions. The FO controller provides a resolution among both the optimistic and adverse impressions of the PID controller.

The cascaded (FOPID/(1+PI)) controller comes from the assimilation of the impression of FO with cascade control.

Riemann – Liouville (R–L) expression for the fractional derivative segment is quantified by equation (11):

$$\alpha D_t^{\alpha} f(t) = \frac{1}{\Gamma(n-\alpha)} \frac{d^n}{dt^n} \int_a^t (t-\tau)^{n-\alpha-1} f(\tau) d\tau \quad (11)$$

where, n−1≤α < n and Γ (·) is the Euler's gamma function.

R–L expression for fractional integral is quantified in equation (12):

$$AD_t^{-\alpha} f(t) = \frac{1}{\Gamma(n)} \int_a^t (t-\tau)^{\alpha-1} f(\tau) d\tau \quad (12)$$

Where aD_t^{α} - fractional operator.

Laplace of R–L expression f is quantified by equation (13):

$$L\{\alpha D_t^{-\alpha} f(t)\} = s^{\alpha} F(s) - \sum_{k=0}^{n-1} s^k \alpha D_t^{\alpha-k-1} f(t)\,|_{t=0} \quad (13)$$

The elementary planning of the FOPID controller is $PI^{\lambda}D^{\mu}$, and the expression of the FOPID controller is quantified by $G_c(s)$ in (14):

$$G_c(s) = K_p + \frac{K_i}{s^{\lambda}} + K_d s^{\mu} \left(\frac{N}{s^{\mu}+N}\right) \quad (14)$$

Where λ and μ are real numbers.

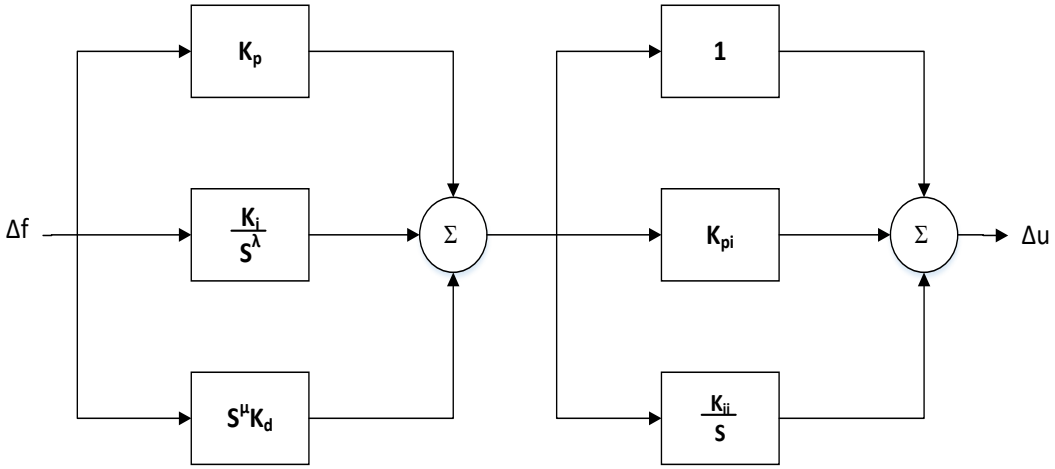

Fig 2: The (FOPID/ (1+PI)) controller

Similarly, the expression of FOPID/ (1+PI) controller C(s) is quantified by equation (15):

$$C(s) = \left(K_p + \frac{K_i}{s^{\lambda}} + K_d s^{\mu} \right) \times \left(1 + K_{pi} + \frac{K_{ii}}{s} \right) \quad (15)$$

Regulating the two chronological progressions consequences in the impression of a multistage structure, which advances the effectiveness of the system concluded as single-loop. The ultimate multistage control system integrates double loops, FOPID and (1+PI). FOPID forms the peripheral controller $C_1(s)$, and (1+PI) is the inside controller $C_2(s)$. The complete transfer function signified by Y(s) in (16):

$$Y(s) = \left[\frac{G_1(s)G_2(s)C_1(s)C_2(s)}{1+G_2(s)C_2(s)+G_1(s)G_2(s)C_{1(s)}C_2(s)} \right] R(s) + \left(\frac{G_1(s)}{1+G_2(s)C_2(s)+G_1(s)G_2(s)C_{1(s)}C_2(s)} \right) d_1(s) \quad (16)$$

3.2 Equilibrium Optimizer (EO):

The EO is enthused by control volume mass balance models, which can evaluate both dynamic and symmetry states. The EO algorithm is designed with high exploratory and exploitative search mechanisms to alter solutions at random [30]. In EO, each particle functions as a search agent or optimization algorithm population, with concentrations randomly updating their locations around equilibrium candidates. This random updating along with a properly defined generation rate term improves EO's exploratory behavior in initial iterations and exploitative search in the final iterations, aiding in local minima avoidance throughout the whole optimization process. The efficiency and effectiveness of EO using quantitative and qualitative metrics have been validated by testing it on a total of 58 mathematical benchmark functions along with three engineering problems [30]. Comparisons with several well-studied, recent, and high-performance optimization algorithms showed a high effectiveness of the proposed EO algorithm in obtaining optimal or near-optimal solutions for the majority of problems investigated.

The generic mass-balance equation is:

$$v\frac{dc}{dt} = QC_{eq} - QC + G \quad (17)$$

C is the concentration, $\frac{dc}{dt}$ is the rate of change of mass, Q is the volumetric flow rate into and out of the control volume, C_{eq} is the concentration at an equilibrium state inside the control volume with no generation, and G denotes the rate of mass generation within the control volume. Taking integration of the above expression, it can be represented as follows:

$$C = C_{eq} + (C_0 - C_{eq}) + \frac{G}{\lambda V}(1 - F) \quad (18)$$

where

$$F = \mathrm{e}^{-\lambda(\mathrm{t}-\mathrm{t0})} \quad (19)$$

and, $\lambda = \text{turnover rate} = \frac{Q}{V}$ (20)

the EO method is described in the steps below:

Step 1: Initializations and function evaluation

The initial population is used by EO to begin the process of optimization. The initial concentrations are calculated using uniform random initialization and based on the number of particles and dimensions in the search space:

$$C_i^{initial} = C_{min} + rand_i\ (C_{max} - C_{min}) \quad (21)$$

For, i =1, 2, 3....., n

where C_{max} refers to the maximum limit of the control variables while C_{min} is the minimum limit. $rand_i$ is a random variable within [0, 1] that evaluate the objective function for each concentration.

Step 2: Assigning the Equilibrium candidates

Based on various trials under various types of testimonials, below are the 4 best particles discovered throughout the search process, as well as additional particles whose concentration is the arithmetic mean of the 4 best particles.

$$C_{eq(avg)} = \frac{C_{eq(1)} + C_{eq(2)} + C_{eq(3)} + C_{eq(4)}}{4} \quad (22)$$

The populations are sorted the four best solutions are captured and their average value to form the pool vector ($C_{eq(pool)}$) is as follows:

$C_{eq(pool)} = \{C_{eq(avg)}, Ceq\ (1), Ceq\ (2), Ceq\ (3), Ceq\ (4)\}$ (23)

Step 3: Main concentration updating

The exponential term (F) is the following term that contributes to the main concentration apprising rule. Two randomly vectors (r, l) are generated and utilized to adjust an exponential factor (F) for updating the concentrations as below:

$$F = a_1\ sign\ (r - 0.5)(e^{-\lambda t} - 1) \quad (24)$$

Where t is given by,

$$t = \left(1 - \frac{T}{Tmax}\right)^{\left(a2\frac{T}{Tmax}\right)} \quad (25)$$

Where a_1 is a fixed value that governs exploring ability. The greater the value of a_1, the greater the exploration capability and, as a result, the poorer the exploitation ability. Likewise, the higher the value of the a_2, the better the exploitation capability and the lower the exploration performance. T_{max} is the maximum iteration number, and T denotes the T^{th} iteration. sign (r - 0.5) controls the direction of the exploration.

Step 4: Generation rate

The most significant element in the suggested method to deliver the meticulous solution by enhancing the exploitation stage is the generation rate, which is demonstrated below:

$$G = G_0\ e^{-k(t-t0)} \quad (26)$$

$$G_0 = GCP\ (C_{eq} - \lambda C) \quad (27)$$

$$GCP = \begin{cases} 0.5\ r_1 & r_2 > GP \\ 0 & r_2 < GP \end{cases} \quad (28)$$

Where r1 and r2 are two random numbers in the range [0,1]. The generation probability (GP) is used to govern the concentration participation probability, which is updated by the generation rate. If GCP = 0, G is also 0, and all of the dimensions of that particle are updated without the usage of a generation rate term. A fair balance between exploration and exploitation is achieved with a GP value equal to 0.5. Using the previous procedures as a guide, the EO's modified equation is as follows:

$$C = C_{eq} + (C - C_{eq}) + \frac{G}{\lambda V}\,(1 - F) \tag{29}$$

4. Result and Analysis

The transfer function model of the MMG system as shown in Fig 1 is used throughout this study. The main source of frequency instability in the MG system is load dynamics and associated uncertainty. Frequency riots are mostly due to load dynamics, wind power fluctuation and solar energy variations in the MG system. To attain stability over system frequencies an EO optimized cascaded fractional order controller (FOPID (1+PI)) is suggested in this study. For the study and analysis of the system dynamics, a step load perturbation (SLP) of 20% at t=0 sec in area 1 & 30% in area 2 is set. The MMG system is given an incremental change in solar irradiation power (shown in Fig. 3) and wind power fluctuation (shown in Fig. 4) to study frequency regulation under various controlled techniques. This section consists of three fundamental phases that will be used to assess the practicality of proposed options in response to frequency awareness in microgrid systems, i.e., Technique stage, Controller stage and Sensitive analysis.

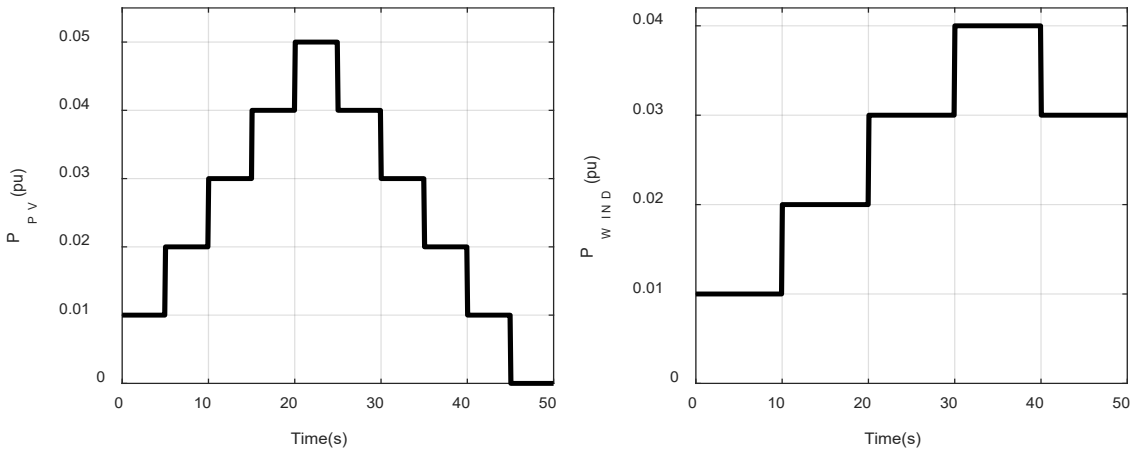

Fig. 3: Variation in solar power irradiation and Wind Power Fluctuation

4.1 Technique Stage

The technique stage emphasizes demonstrating the superiority of the proposed EO over GA, SCA and PSO performances. Initially, the PID controller is incorporated in both areas of the MMG system. In the next step, the system is tuned using four intelligent optimization techniques i.e., GA, SCA, PSO and the proposed EO algorithm. The convergence curves of EO, SCA, PSO and GA for the PID controller are provided in Fig. 4. The dynamic responses of the system obtained using the PID controller are shown in Fig. 5(a) - (c). It was observed that the performance of the system increases steadily as we approach from GA to EO algorithm. In the subsequent series of

cases, the PID controller is replaced with the FOPID and FOPID/(1+PI) controller and its dynamic response is recorded. The dynamic response under the incorporation of FOPID and FOPID/(1+PI) controller is shown in Fig. 5(d)-(f) and Fig. 5(g)-(i) respectively. The response as shown in Fig. 6 clearly states that the most optimum performance was obtained when the EO algorithm was used with the display of better settling time, peak overshoot and undershoot. The optimum values of controller parameters are presented in Table 2 and performance parameters in Table 3. The ITAE values comparison of the different affected algorithms used i.e., GA, PSO, SCA and EO are portrayed in Fig. 6. The ITAE value also confers the same conclusion about the supremacy of the EO algorithm over its counterparts by showing a decreasing trend in its value from GA to EO. Thus, it can be concluded that the EO technique is providing better system performance in stabilizing the frequency and tie-line power in the MMG system. Hence, for further analysis, the EO algorithm will be considered.

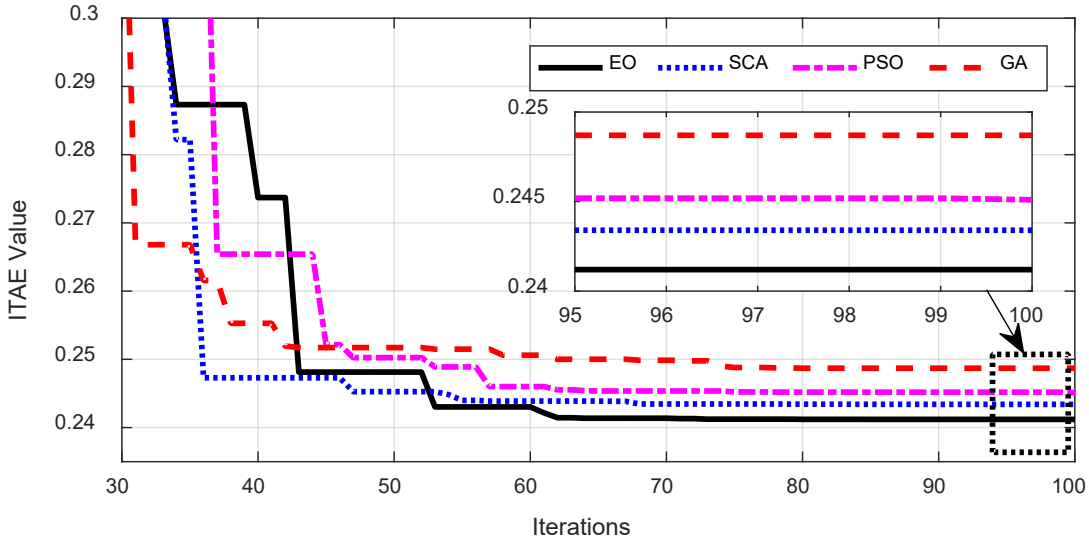

Fig. 4 Convergence curves of EO, SCA, PSO and GA for PID controller

Table 2: Optimized Parameters of Controllers under different conditions

ALGORITHM	CONTROLLER	OPTIMIZED PARAMETERS OF CONTROLLER AREA1							AREA2						
		K_{P11}/K_{P1}	K_{P12}	K_{I1}	K_{I12}	K_{D1}	λ_1	μ_1	K_{P21}/K_{P2}	K_{P22}	K_{I2}	K_{I22}	K_{D2}	λ_2	μ_2
GA	**PID**	0.4519	-0.0152	1.9900	-0.2766	0.1800	-	-	1.9900	-1.9656	1.9600	-1.9760	0.0200	-	-
	FOPID	1.4678	-0.0152	1.8565		0.1319	1.2438	1.4554	1.9591	-1.9656	1.7034	-1.9760	1.5277	1.5114	0.3503
	FOPID/(1+PI)	1.5125	-0.0152	-0.2786	1.9452	0.0462	0.1818	1.0675	0.6690	1.9656	1.4403	1.9760	1.5036	0.7648	0.2023
PSO	**PID**	0.6519	-0.0152	1.9800	-0.2766	0.1707	-	-	2.1000	-1.9656	1.9600	-1.9760	0.0200	-	-
	FOPID	0.9286	-0.0152	1.9800	-0.2766	0.3714	1.0283	0.9713	0.5106	-1.9656	1.9452	-1.9760	1.8684	1.3744	0.1665

SCA	**FOPID/(1+PI)**	0.5414	1.5657	1.8478	1.9978	0.1496	0.8454	1.0463	1.9800	-0.5155	1.9834	1.9760	0.4096	0.0486	1.4031
	PID	0.7804	-1.9800			0.1786			1.9900		1.9600		0.0630		
	FOPID	1.9740	-1.9800			0.1580	0.9992	1.2735	1.9900		1.9600		0.0200	1.3220	1.4654
EO	**FOPID/(1+PI)**	1.8421	1.1448	1.7684	1.9416	0.6502	0.8855	0.6128	1.7116	1.8825	1.7472	1.4895	1.8114	0.9072	0.1579
	PID	0.8697	-1.9800			0.2184			1.2900		1.9600		0.1471		
	FOPID	1.7652	-1.9800			0.3538	0.9794	1.2602	1.9900		1.9600		1.9860	1.5961	0.1557
	FOPID/(1+PI)	2.1001	1.9230	1.9880	1.9978	1.9870	0.2796	0.6594	1.9800	1.9870	1.9910	1.9760	1.9860	1.3121	0.2729

Table 3: Transient Response Parameters and Performance Index *J* (ITAE)

ALGORITHM	**CONTROLLER**	**TRANSIENT RESPONSE PARAMETERS**						**PERFORMANCE INDEX *J* (ITAE)**
		OVERSHOOT ($\times10^{-3}$), (pu)			**UNDERSHOOT ($\times10^{-3}$), (pu)**			
		Δf_1	**Δf_2**	**ΔP_{tie}**	**Δf_1**	**Δf_2**	**ΔP_{tie}**	
GA	**PID**	5.091	0.244	0.545	-22.04	-2.663	-18.17	0.2487
	FOPID	4.886	0.054	1.001	-12.96	-1.236	-15.97	0.2300
	FOPID/(1+PI)	1.754	0.026	0.213	-37.16	-1.245	-17.53	0.1458
PSO	**PID**	3.839	0.063	0.519	-22.39	-1.586	-16.20	0.2451
	FOPID	2.211	0.099	0.452	-14.30	-0.612	-13.19	0.2127
	FOPID/(1+PI)	0.797	0.053	1.006	-0.091	-0.043	-0.090	0.0751
SCA	**PID**	3.086	0.092	0.510	-21.34	-1.650	-14.79	0.2434
	FOPID	2.294	0.058	0.393	-13.12	-0.920	-10.68	0.2053
	FOPID/(1+PI)	0.490	0.033	0.606	-12.37	-0.440	-0.090	0.0573
EO	**PID**	2.488	0.082	0.531	-18.03	-1.311	-13.37	0.2412
	FOPID	1.802	0.040	0.265	-7.613	-0.582	-10.94	0.1873
	FOPID/(1+PI)	0.059	0.016	0.077	-5.597	-0.053	-1.260	0.0483

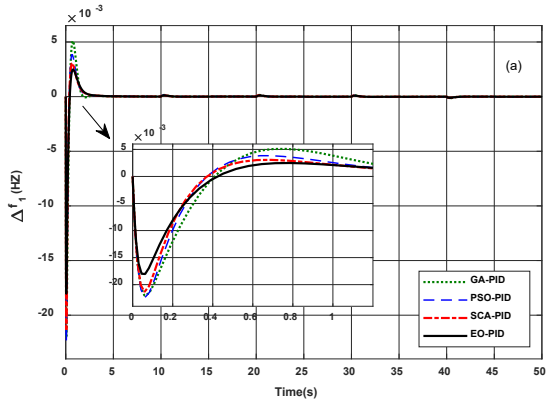
(a)
Δf1 (HZ)
Time(s)
GA-PID
PSO-PID
SCA-PID
EO-PID

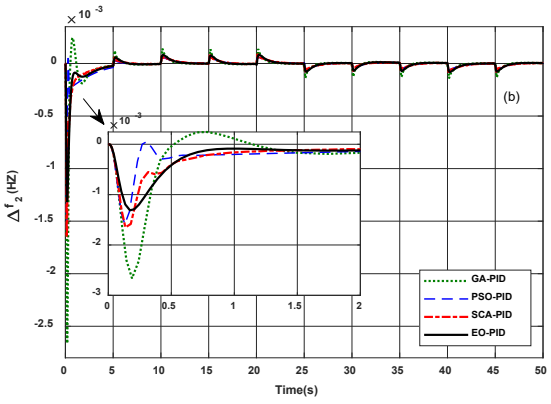
(b)
Δf2 (HZ)
Time(s)
GA-PID
PSO-PID
SCA-PID
EO-PID

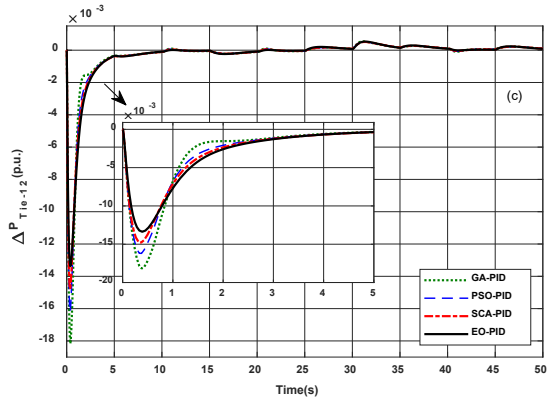
(c)
ΔPTie-12 (p.u.)
Time(s)
GA-PID
PSO-PID
SCA-PID
EO-PID

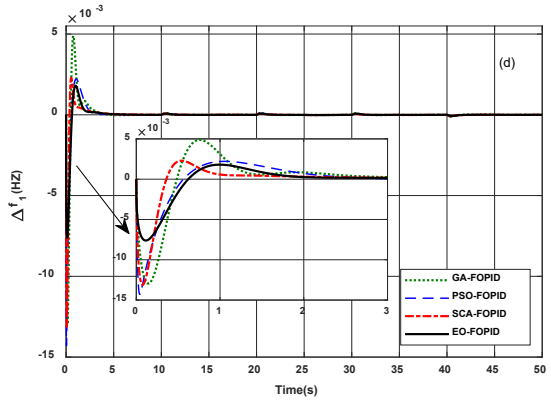
(d)
Δf1 (HZ)
Time(s)
GA-FOPID
PSO-FOPID
SCA-FOPID
EO-FOPID

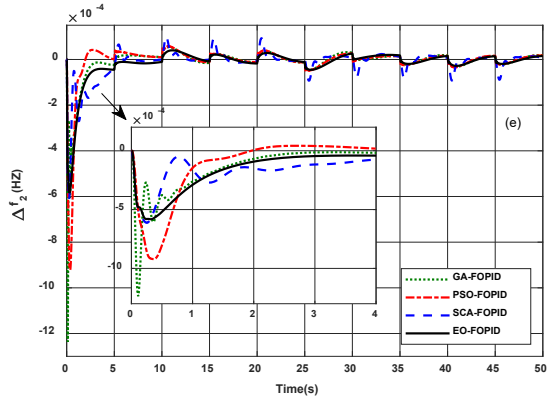
(e)
Δf2 (HZ)
Time(s)
GA-FOPID
PSO-FOPID
SCA-FOPID
EO-FOPID

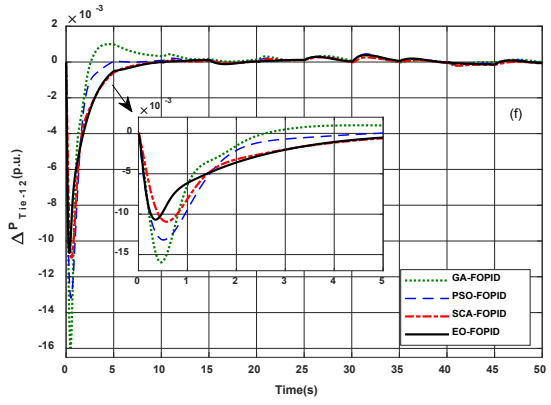
(f)
ΔPTie-12 (p.u.)
Time(s)
GA-FOPID
PSO-FOPID
SCA-FOPID
EO-FOPID

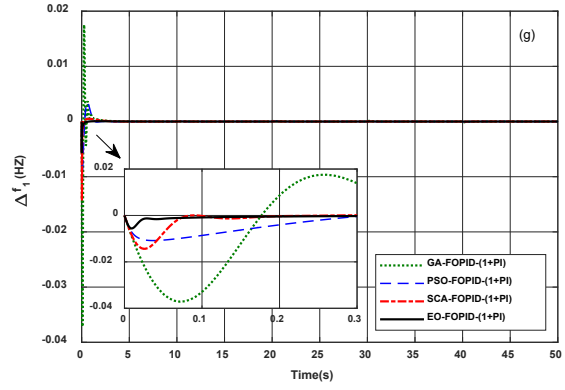
(g)
Δf1 (HZ)
Time(s)
GA-FOPID-(1+PI)
PSO-FOPID-(1+PI)
SCA-FOPID-(1+PI)
EO-FOPID-(1+PI)

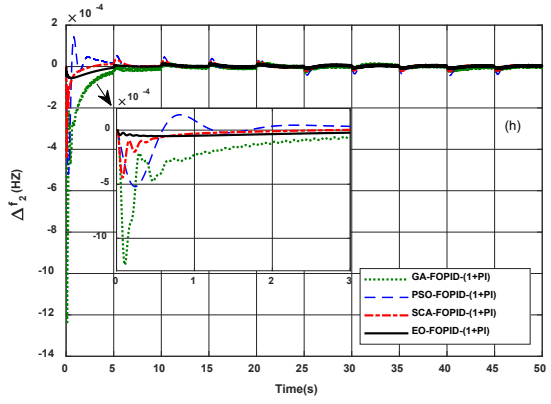
(h)
Δf2 (HZ)
Time(s)
GA-FOPID-(1+PI)
PSO-FOPID-(1+PI)
SCA-FOPID-(1+PI)
EO-FOPID-(1+PI)

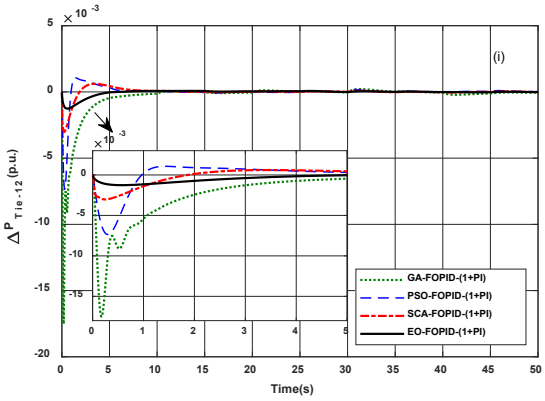

Fig 5: Performance of MMG with (a)-(c) PID, (d)-(f) FOPID, (g)-(i) FOPID(1+PI) using GA, PSO, SCA and EO methods.

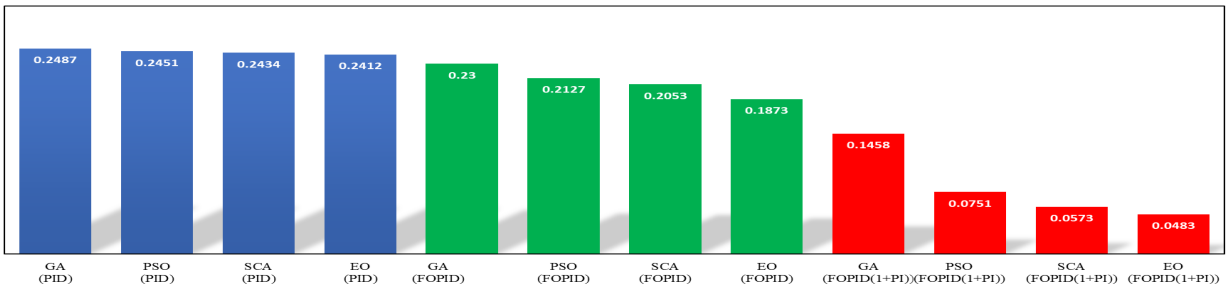

Fig 6: Fitness mapping of various approaches

4.2 Controller Stage

This case study deals with demonstrating the supremacy of the proposed FOPID/(1+PI) controller over the FOPID and PID controller for frequency regulation of an MMG system. The EO algorithm has already been justified as a superior algorithm in section 4.1. In this section, the EO algorithm will only be used to optimize the controller parameters. Initially, the two-area MG is incorporated with the PID controller and the dynamic response of the system is recorded. In subsequent stages, the PID controller is replaced with the FOPID and FOPID/(1+PI) controller and the dynamic response is recorded. Fig. 7(a)-(c) shows the comparison of dynamic response with the three controllers obtained in area 1, area 2 and the tie-line. Fig. 8 shows the performance index values of the three controllers. The optimal gain parameters of the controllers and transient response parameters with ITAE values under different conditions are assembled in Table 2 and Table 3 respectively.

The suggested EO optimized cascaded FOPID/(1+PI) controller enhances system dynamic responses greatly under various uncertainties, as illustrated in Fig. 7, and is proven to be more effective in terms of obtaining the least settling time, reduced peak overshoot, and undershoot of the response. Moreover, the ITAE values being the representation of the increased performance of the MMG also suggest the same supremacy of the (FOPID/(1+PI)) controller. As a result, it can be concluded that the proposed approach (EO: FOPID/(1+PI)) provides a satisfactory stable and robust control.

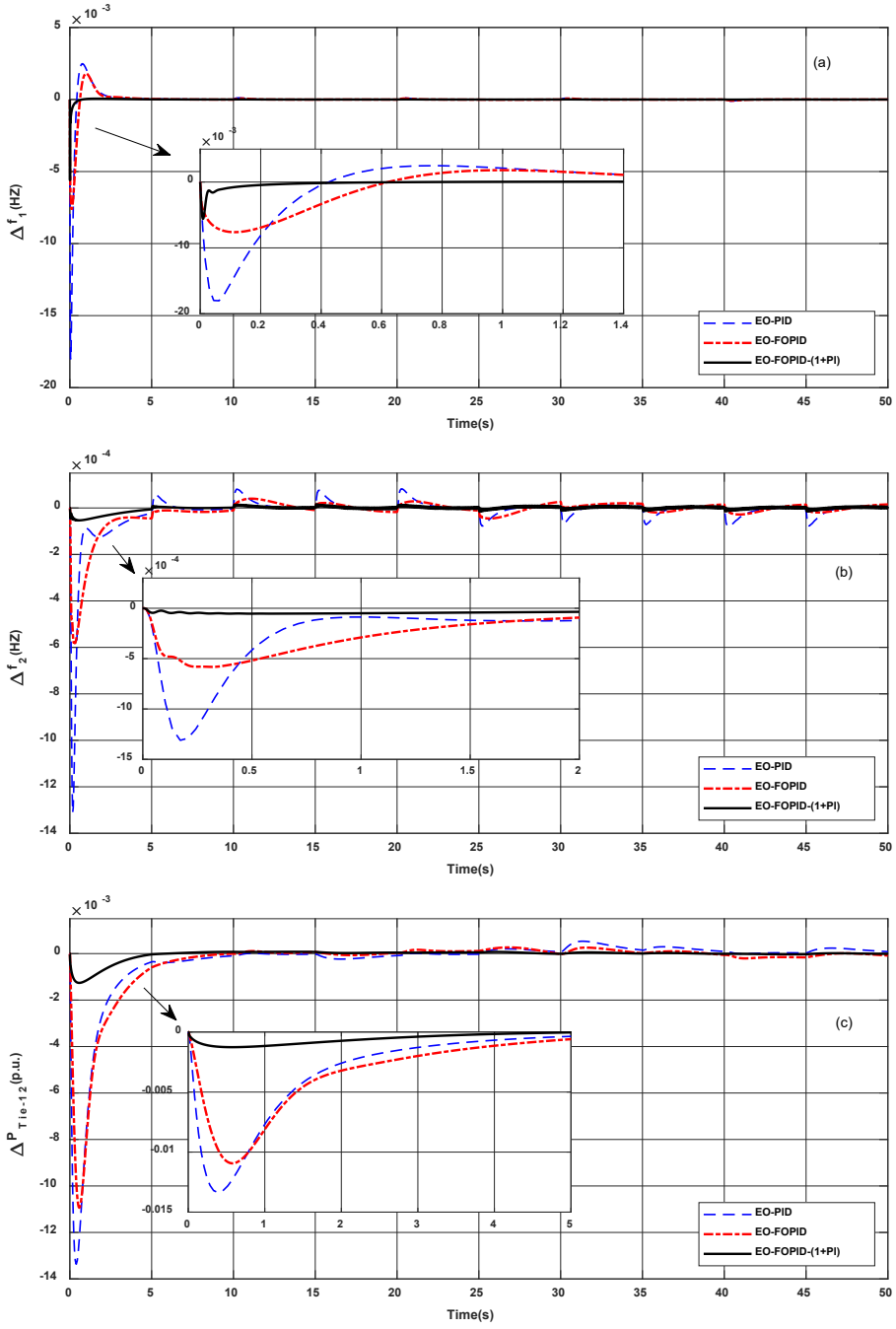

Fig 7: Dynamic response of the MMG in (a) Area-1, (b) Area-2, and (c) Tie-Line.

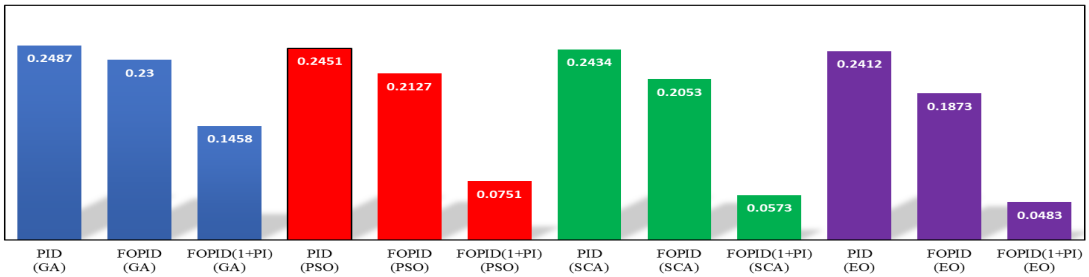

Fig 8: Fitness mapping of various controller approaches

4.3 Sensitivity Analysis

Sensitivity and robustness tests show that the suggested frequency controller for the MMG system is effective. Different sensitive analyses are used to corroborate the robustness of the proposed EO based FOPID/(1+PI) controller. The sensitivity study of the EO: FOPID/(1+PI) controller refers to the impact of changes in the MMG system parameter on controller performance.

4.3.1 Robustness Against Variation of Time Constant

In this section, the sensitivity analysis is progressed with the variation of the time constant of different components of the MMG system like WTG, PV, MT, FC, EV, UC and DEG. To examine system performance under the suggested EO: FOPID/(1+PI) controller, the system parameters are regulated with 40% reduced and 40% increased from their nominal values in this study. Fig. 9 shows the response of a deviation in system frequency. The changes in objective function values are shown in Table 4, which are in near 5% tolerance and slightly more. All of the responses were obtained without changing the proposed EO: FOPID/(1+PI) controller's optimal parameters. The responses are simple overlapping or little variation under wide manipulation of system parameters, as shown in Fig. 9. This shows that, in the context of unaltered controller parameters, broad system parameter adjustment has little impact on system performance. With the extensive change of system parameters, a critical study of all dynamic responses suggests that to acquire the desired performance, there is no requirement for repeated retuning of the controller parameters.

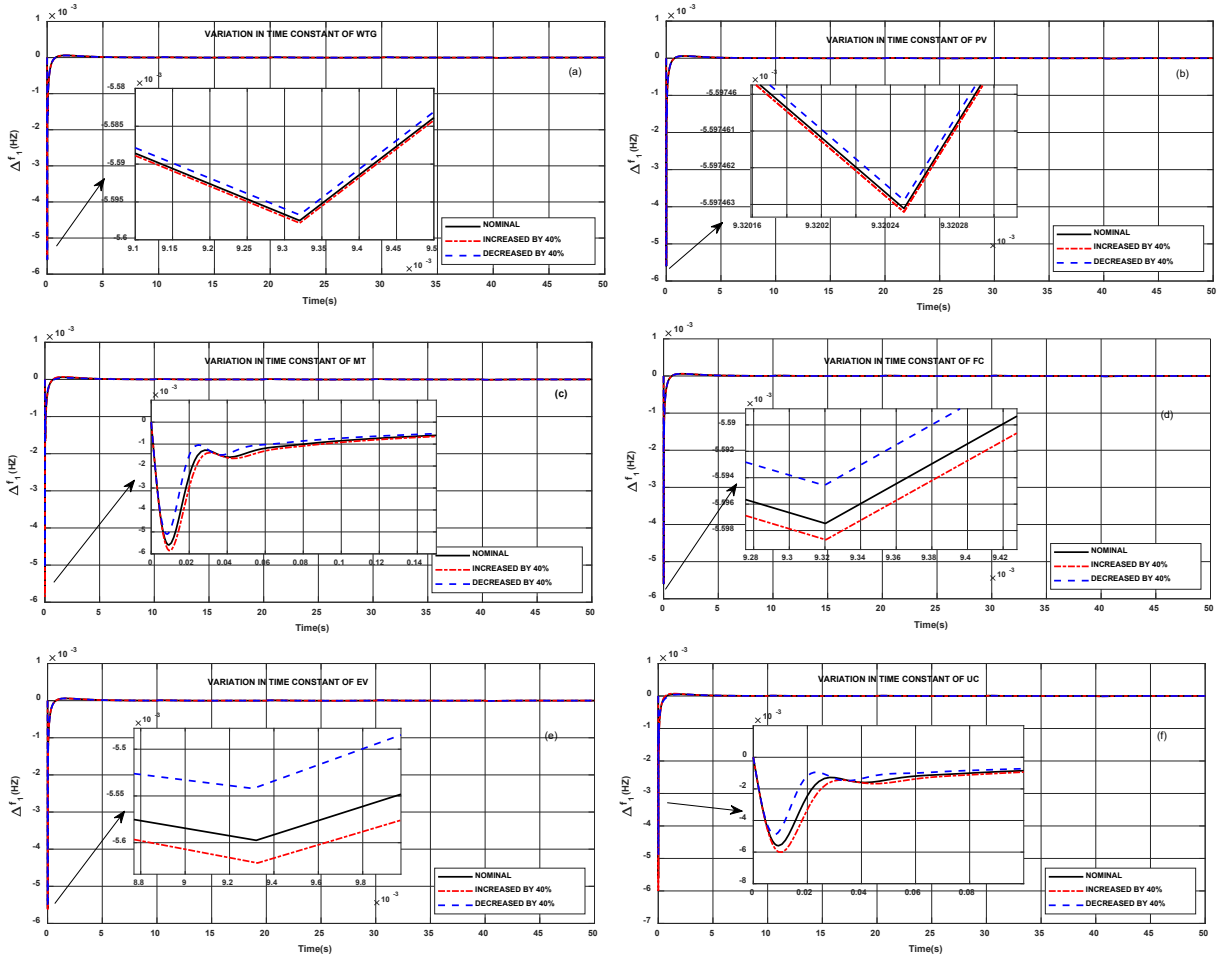

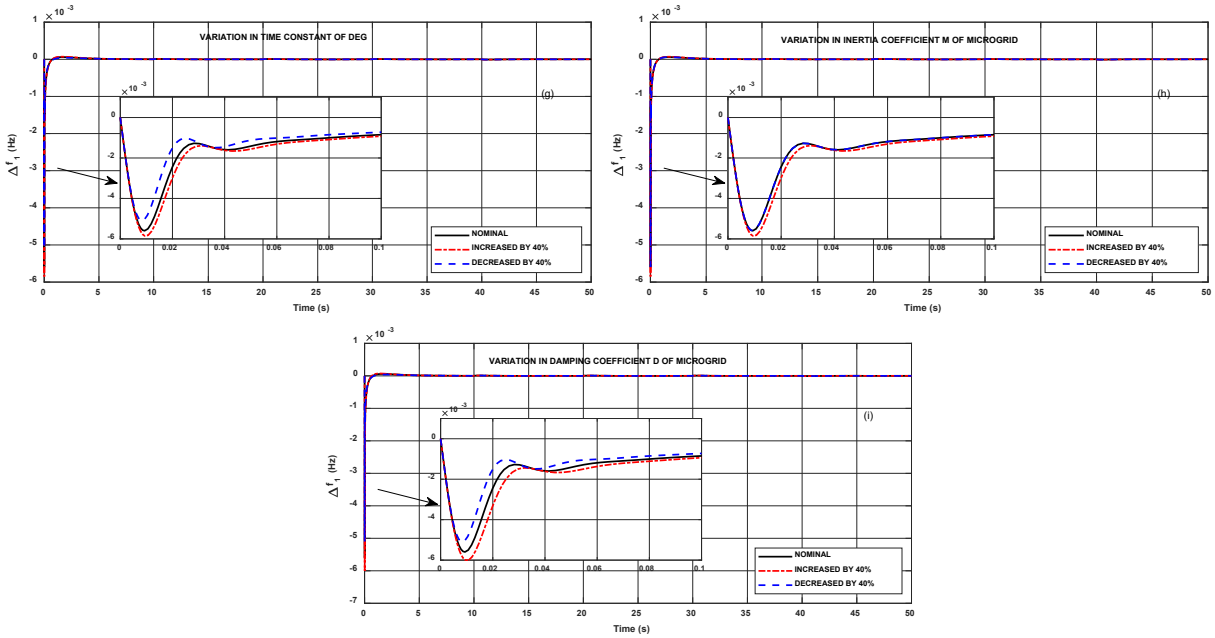

Fig 9: Dynamic response under the changed parametrization of (a) WTG, (b) PV, (c) MT, (d) FC, (e) EV, (f) UC, (g) DEG, (h) M and (i) D

Table 4: Percentage variation in Performance Index J under the regulation of the time constant of different components of MMG.

Components	Variation of Time Constant of System Components	ITAE	%Change from Nominal Value
WTG	40% increase	0.0492	1.86%
	40% decrease	0.0475	-1.65%
PV	40% increase	0.0520	7.66%
	40% decrease	0.0470	-2.69%
MT	40% increase	0.0502	3.93%
	40% decrease	0.0476	-1.44%
FC	40% increase	0.0484	0.20%
	40% decrease	0.0482	-0.20%
EV	40% increase	0.0488	1.04%
	40% decrease	0.0475	-1.65%
UC	40% increase	0.0486	0.62%
	40% decrease	0.0481	-0.41%
DEG	40% increase	0.0503	4.14%
	40% decrease	0.0475	-1.65%
M	40% increase	0.0503	4.14%
	40% decrease	0.0463	-4.14%
D	40% increase	0.0509	5.39%
	40% decrease	0.0458	-5.17%

4.3.2 Compatibility Assessment

The suggested system's flexible qualities are evaluated against various components by detaching one component at a time and evaluating their performance measurements (ITAE). The five components chosen are MT, FC, EV, UC and DEG due to their presence in both the area of the

MMG. These four components are independently detached and the performance of the system under the detachment condition is observed. All of the responses were calculated without modifying the controllers' optimal parameters as shown in Table 2, which were determined using the EO algorithm. While Table 5 specifies the respective performance index (ITAE) values obtained with the elimination of different components of MMG, Fig. 10 specifies their respective dynamic response.

Table 5: Performance Index J obtained during the elimination of different components of MMG

Components Removed	**Performance Index (ITAE)**		
	EO: PID	**EO: FOPID**	**EO: FOPID(1+PI)**
NOMINAL (No Removal)	0.2412	0.1873	0.0483
MT	0.3812	0.2953	0.0730
FC	0.2425	0.1882	0.0481
EV	0.2380	0.1894	0.0478
UC	0.3258	0.2548	0.0652
DEG	0.3862	0.3009	0.0730

From the results specified in Table 5 and Fig 10, it is noticed that change in the performance of the system is least in the case of EO: FOPID(1+PI) compared to the EO: PID and the EO: FOPID. The disconnection of MT, FC, EV, UC and DEG decreases the performance index (ITAE) values from their nominal value by approximately 58.04%, 0.53%, 1.32%, 35.07% and 60.11% in EO: PID, 57.66%, 0.48%, 1.12%, 36.03%, and 60.65% in EO: FOPID and 51.1%, 0.41%, 1.03%, 34.98%, and 51.13% in FOPID-(1+PI), respectively. Thus, justifying the robustness of the proposed EO optimized FOPID(1+PI) controller.

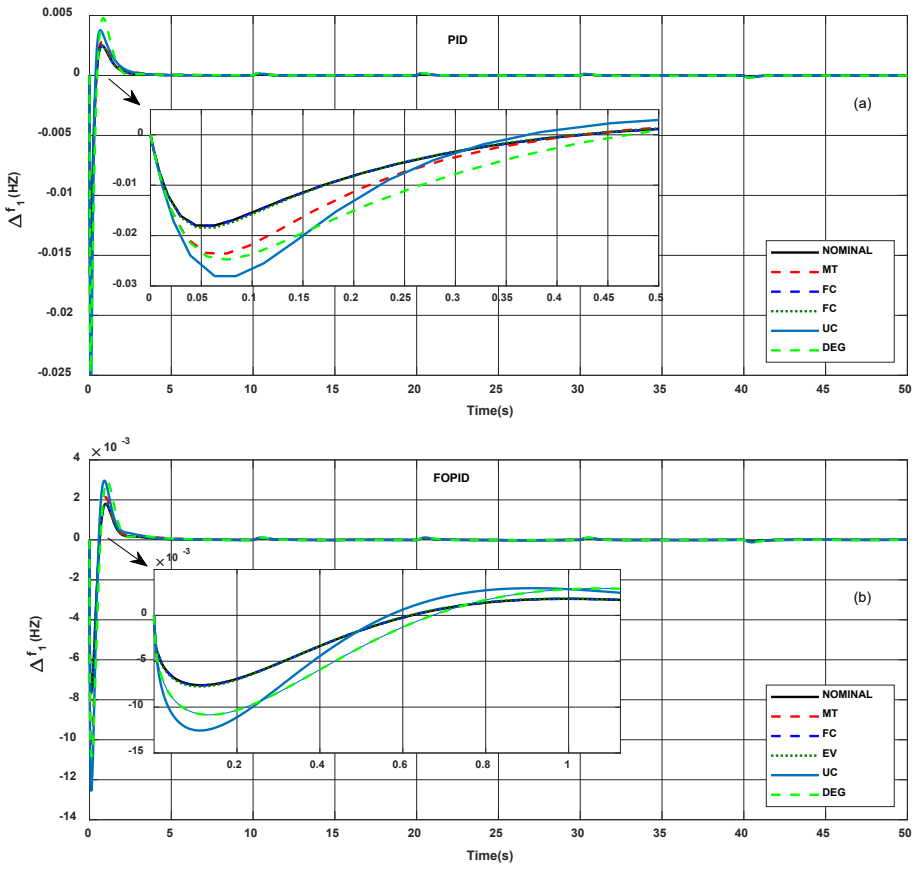

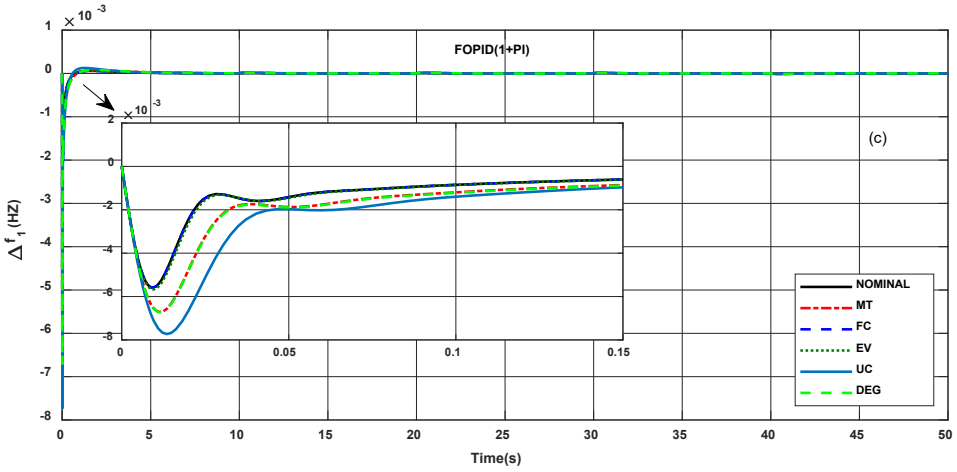

Fig 10: Dynamic responses obtained during the elimination of different components, when (a) PID, (b) FOPID, and (c) FOPID(1+PI) controller respectively is incorporated in the MMG.

4.3.3 Time Delay Assessment

The commutating channel to the EO-optimized FOPID(1+PI) controller can establish a time-varying or fixed delay which may degrade the MMG performance adversely. Hence, the tolerance of the time delay zone has to be measured for the organization's optimal control scheme for frequency regulation of the MMG. In this regard, the EO: FOPID(1+PI) approach is validated with probable time delays to measure the robustness of controller performance. The effect of time delay in frequency regulation is demonstrated in Fig. 11. The controllers' optimal parameters as shown in Table 2 are considered with 5ms, 10ms and 15ms time delay for the study. The error in ITAE value enhanced by 3.45% for a 5ms delay, 5.82% for a 10ms delay and 6.92% for a 15ms delay respectively. As it is observed from Fig. 10 time delays lead to enhanced oscillations exhibited but the proposed EO: FOPID(1+PI) approach is quite able to provide appropriate damping to these oscillations reflecting robustness.

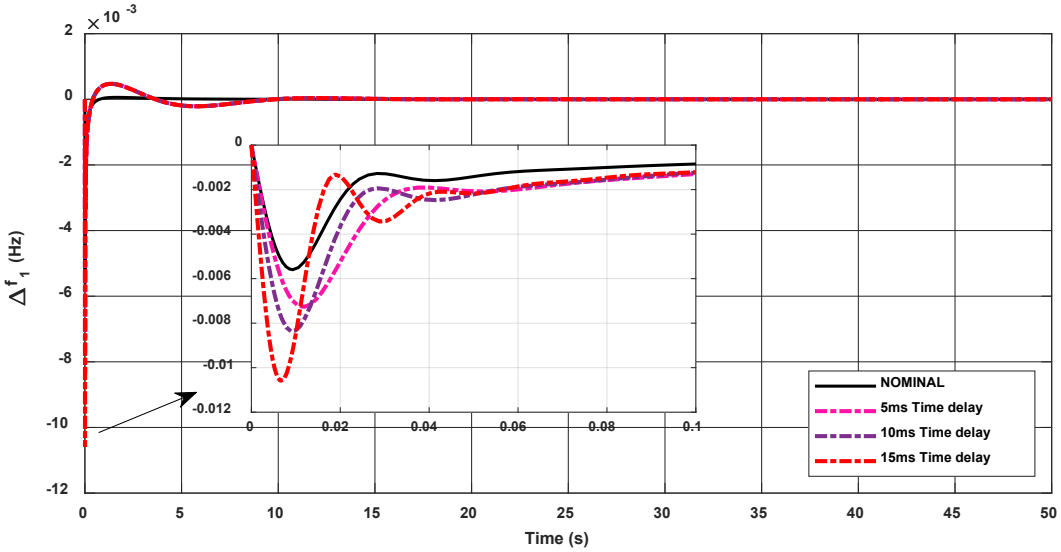

Fig 11: Dynamic frequency responses for MG1 with the introduction time delays

Conclusion

In this investigated work, an original effort has been executed to employ an EO algorithm for load frequency control of two-area MG. The performance of EO algorithms is related to supplementary intelligent schemes like SCA, PSO and GA. It is observed that for the same system under investigation, the EO method outperforms the GA, PSO and SCA algorithms. In the subsequent phase, the projected EO is utilized to optimize the controllers to deal with the LFC of the MMG system. The proposed approach EO-based FO multi-stage controller completely outperforms in terms of various dynamic responses. Additionally, the suggested EO-FOPID/ (1+PI) controller's robustness is verified using various sensitivity analyses.

The research outcomes of the above investigations are summarized below:

1) For the technique stage, it has been identified that the enrichment in ITAE value with the anticipated EO algorithm as related to SCA, PSO and GA, are 15.7%, 35.6% & 66.8%, respectively, while taking (FOPID/(1+PI)) controller. Similar improvements are also observed, even in the case when PID and FOPID controllers are implemented.
2) For the technique stage, the augmentation in ITAE value with anticipated EO-FOPID controller linked to EO-FOPID and EO-PID, controllers 74.2% & 79.9% respectively.
3) Finally, various robustness study is accomplished such as system parameter alternation, removal of micro sources and communication delay to the controllers to justify the sturdiness of the anticipated EO tuned FOPID/ (1+PI) controller.

Reference

[1] O. Palizban and K. Kauhaniemi, “Hierarchical control structure in microgrids with distributed generation: Island and grid-connected mode”, Renewable and Sustainable Energy Reviews, 2015, 44: 797-813.

[2] D. Wu, F. Tang, T. Dragicevic, J. C. Vasquez and J. M. Guerrero, “Autonomous Active Power Control for Islanded AC Microgrids with Photovoltaic Generation and Energy Storage System”, IEEE Transactions on Energy Conversion, 2014, 29(4): 882-892, doi: 10.1109/TEC.2014.2358612.

[3] O.I. Elgerd, “Electric Energy Systems Theory: An Introduction”, 2nd ed., New Delhi: Tata McGraw-Hill, 1983.

[4] W. Tan, Z. Xu., “Robust analysis and design of load frequency controller for power systems”, Electric Power Systems Research, 2009, 79(5):846–853.

[5] N. Hasan, “Design and analysis of pole-placement controller for interconnected power systems”, International Journal of Emerging Technology and Advanced Engineering, 2012, 2(8):212–217.

[6] W. Tan, H. Zhou, “Robust analysis of decentralized load frequency control for multi-area power systems”, International Journal of Electrical Power & Energy Systems, 2012, 43(1):996–1005.

[7] H.A. Yousef, K. AL-Kharusi, M.H. Albadi, N. Hosseinzadeh, “Load frequency control of a multi-area power system: an adaptive fuzzy logic approach”, IEEE Transactions on Power Systems, 2014, 29(4):1822–1830.

[8] D. Xu, J. Liu, X. Yan and W. Yan, “A Novel Adaptive Neural Network Constrained Control for a Multi-Area Interconnected Power System with Hybrid Energy Storage”, IEEE Transactions on Industrial Electronics, 2018, 65(8): 6625-6634.

[9] P.C. Nayak, R.C. Prusty, and S. Panda, "Adaptive fuzzy approach for load frequency control using hybrid moth flame pattern search optimization with real-time validation", Evolutionary Intelligence, 2022, 1-16.
[10] S. Das, S. Panda, "An optimized fractional order cascade controller for frequency regulation of power system with renewable energies and electric vehicles", Energy Systems, 2021, doi: 10.1007/s12667-021-00461-9.
[11] C. A. Monje, Y. Q. Chen, B. M. Vinagre, D. Xue, and V. Feliu, "Fractional-order Systems and Controls", London: Springer-Verlag, 2010.
[12] I. Pan, and S. Das, "Intelligent fractional order systems and control: An Introduction (Studies in Computational Intelligence)", 438, Berlin, Germany: Springer-Verlag, 2013.
[13] I. Pan, and S. Das, "Fractional order fuzzy control of hybrid power system with renewable generation using chaotic PSO", ISA Transactions, 2016, 62: 19–29.
[14] A. J. Khakshour and M. A. Khakshour, "Model reference fractional order control using type-2 fuzzy neural networks structure: implementation on a 2-dof helicopter", Neuro Computing, 2016, 193: 268–79e.
[15] I. Pan and S. Das, "Fractional order AGC for distributed energy resources using robust optimization", IEEE Transactions on Smart Grid, 2016, 7(5): 2175–86.
[16] Y. Arya, "Effect of energy storage systems on automatic generation control of interconnected traditional and restructured energy systems", International Journal of Energy Research, 2019, 43(12): 6475–93.
[17] H. K. Abdulkhader, J. Jacob, and A. T. Mathew, "Fractional order lead-lag compensator-based multi-band power system stabiliser design using a hybrid dynamic GA-PSO algorithm", IET Generation, Transmission & Distribution, 2018, 12(13): 3248–60.
[18] K. Nosrati, H. R. Mansouri, and S. Saboori, "Fractional order PID controller design of frequency deviation in a hybrid renewable energy generation and storage system", CIRED - Open Access Proceedings Journal, 2017, 1: 1148–52.
[19] I. Pan, and S. Das, "Kriging based surrogate modelling for fractional order control of microgrids", IEEE Transactions on Smart Grid, 2015, 6(1): 36–44.
[20] P.C. Nayak, R.C. Prusty and S. Panda, "Grasshopper optimisation algorithm of multistage PDF + (1 + PI) controller for AGC with GDB and GRC nonlinearity of dispersed type power system", International Journal of Ambient Energy, 2022, 43(1): 1469-1481, doi: 10.1080/01430750.2019.1709897.
[21] A.E. Milani and B. Mozafari, "Genetic algorithm based optimal load frequency control in two area interconnected power system", Global Journal of Technology and Optimization, 2011, 2:6–10.
[22] R.K. Khadanga and J.K. Satapathy, "Time delay approach for PSS and SSSC based coordinated controller design using hybrid PSO-GSA algorithm", International Journal of Electrical Power & Energy Systems, 2015, 71:262–273.
[23] A.Y. Abd-Elaziz and E.S. Ali, "Cuckoo search algorithm-based load frequency controller design for nonlinear interconnected power system", International Journal of Electrical Power & Energy Systems, 2015, 73C:632–643.
[24] S.M. Abd-Elazim and E.S. Ali, "Load frequency controller design of a two-area system composing of PV grid and thermal generator via firefly algorithm", Neural Computing and Applications, 2018, 30: 607–616.
[25] P.C. Nayak, B. P. Nayak, R.C. Prusty, and S. Panda, "Sunflower optimization based fractional order fuzzy PID controller for frequency regulation of solar-wind integrated power

system with hydrogen aqua equalizer-fuel cell unit", Energy Sources, Part A: Recovery, Utilization, and Environmental Effects, 2021, 45: 1-19.
[26] P.C. Nayak, U.C. Prusty, R.C. Prusty, and S. Panda, "Imperialist competitive algorithm optimized cascade controller for load frequency control of multi-microgrid system", Energy Sources, Part A: Recovery, Utilization, and Environmental Effects, 2021, 45: 1-23.
[27] P.C. Nayak, S. Mishra, R.C. Prusty, and S. Panda, "Hybrid whale optimization algorithm with simulated annealing for load frequency controller design of hybrid power system", Soft Computing, 2023, doi:10.1007/s00500-023-09072-1.
[28] J. Wu and F. Yang, "A dual-driven predictive control for photovoltaic-diesel microgrid secondary frequency regulation", Applied Energy, 2023, 334: 1-9.
[29] A. H. Yakout, K. M. AboRas, H. Kotb, M. Alharbi, M. Shouran and A. S. Bdereddin, "A Novel Ultra Local Based-Fuzzy PIDF Controller for Frequency Regulation of a Hybrid Microgrid System with High Renewable Energy Penetration and Storage Devices", Processes, 2023, 11:1-22.
[30] A. Faramarzi, M. Heidarinejad, B. Stephens and S. Mirjalili, "Equilibrium optimizer: A novel optimization algorithm", Knowledge-Based Systems, 2020, 191: 105190.